Available online at www.sciencedirect.com
SCIENCE DIRECT
Polymer 46 (2005) 8355–8365
polymer
www.elsevier.com/locate/polymer

Structure of bimodal and polydisperse polymer brushes in a good solvent studied by numerical mean field theory

Georgios Kritikos, Andreas F. Terzis*

Department of Physics, University of Patras, GR 26504 Patras, Greece

Received 20 April 2005; received in revised form 21 June 2005; accepted 21 June 2005
Available online 20 July 2005

Abstract

We apply a lattice-based self-consistent mean field theory in order to investigate poly-disperse polymer brushes dissolved in good solvent. The systems investigated consist of asymmetric poly(dimethylsiloxane)–polystyrene di-block copolymers near air–ethylbenzoate interface and of diblock copolymer polystyrene–poly(ethyl oxide) deposited on a air–water interface. Our results have been compared to experimental data from neutron reflectivity experiments and have shown very good agreement. We have also systematically studied the structure of the bi-disperse and tri-disperse brush for various values of the molar fraction of the chains and of the overall surface densities. In addition, we have investigated the behavior of the brushes in other type of solvents.

Keywords: Polydisperse molecular weight distribution; Polymer brush in good solvent; Mean-field theory

1. Introduction

Chains anchored by one end to a surface or an interface, are called polymer brushes [1–6]. They provide practical means for modifying interfacial properties. Strong overlap among neighboring chains is observed once the distance between grafted points is small compared to the macromolecular chain dimensions. Hence, the chains deform and stretch in the direction perpendicular to the interface. They are often formed by adsorption from solution, i.e. by bringing a solution containing end-functionalized chains into contact with an interacting surface. The ends can either be chemically attached (quite high binding energy [7,8]) or physi-adsorbed [9–11]. The adsorbing, functional end could be a reactive group, or the immiscible block of a copolymer [12–17].

Initial theoretical and experimental studies of polymer brushes, were concentrated on monodisperse polymers. However, polydispersity, which is often an unavoidable feature of polymer systems (most commercial polymers has a broad molecular weight distribution), has been shown to affect the brush structure [18–24]. The properties of bimodal polymer brushes were first explored with analytical self-consistent mean field (SCF) methods, valid in the limit of strong stretching and for infinite molecular weight [19,20]. Dan and Tirrel [23] have examined prototype bimodal brushes in great detail by means of numerical self-consistent mean field (nSCF) calculations. An understanding of the relationship between the molecular weight distribution and the brush properties is thus essential for purely scientific reasons and for engineering applications (i.e. tailoring the brush structure according to specific needs).

In this paper, we systematically investigate realistic polydisperse polymer brushes mainly in a good solvent. In Section 2, we present the theoretical backgrounds and explain the numerical self-consistent field method. In next sections we mainly investigate bimodal systems previously studied by neutron reflectivity experiments [25–28]. We also investigated trimodal (tri-disperse) distributions and polydisperse brushes in other type of solvents. We end our presentation with the conclusions and proposals for future studies in Section 5.

* Corresponding author. Tel./fax: +30 2610 997618.
E-mail address: terzis@physics.upatras.gr (A.F. Terzis).

0032-3861/$ - see front matter © 2005 Elsevier Ltd. All rights reserved.
doi:10.1016/j.polymer.2005.06.076

2. The self-consistent field model

In the present theoretical investigation, we apply a

self-consistent mean field theory in order to describe our polymeric system (i.e. a polymeric solution near a surface). The SCF theory was originally developed for bulk polymeric systems [29] and later developed by Dolan and Edwards [30,31] to treat polymers in inhomogeneous environments. The basic idea of this method is to solve for the Green functions propagators describing the local density of a random walk representation of a polymer chain in the presence of the mean field imposed by the repulsive and attractive interactions between all macromolecular chains. This mean field is a function of the local density, which in turn is determined, self-consistently, by the average value obtained from the Green functions propagators. One of the most powerful versions of this approach is the lattice version, developed by Scheutjens and Fleer [32–35].

The self-consistent equations have an analytical solution for a particular limit, usually referred to as the classical limit [35]. The analytical theories [36–44] took advantage of the fact that in a system in which polymers are strongly stretched as in a brush, fluctuations around the most probable, or 'classical' paths are small and can be ignored to a first approximation. In the analytical self-consistent field (aSCF) theories the mutual interaction of the polymer chains is represented by a mean-field (referred as 'Kinematic' potential) that gives rise to a non-uniform stretching of the chains [19]. The conformations of polymer chains are similar to the flight path of a particle starting at rest at the location of the free end and being accelerated in a field toward the 'bottom' of the brush. Exploiting the property that the chain ends are located everywhere, it has been shown that the mean-field potential is harmonic [19]. In addition aSCF theories have been extended in order to study dense polymer brushes following a bimodal molecular weight distribution [20,40]. For bimodal brush, it has been revealed that the ends of the shorter and the longer chains segregate into separate regions [20,40].

The self-consistent mean-field lattice model developed by Scheutjens and Fleer has been used to describe polymer melts and polymeric solutions near a solid substrate, polymers chemically attached to the substrate, rings, branched chains, copolymers and multi-component polymeric systems [6].

A three-dimensional (xyz) lattice of simple symmetry is assumed. The substrate is placed parallel to the xy plane; the resulting lattice layers are numbered starting from the layer next to the surface ($z=1$) and ending at a layer ($z=M$) where the presence of the substrate has negligible effect. Each lattice site has Z (the coordination number) neighboring sites, a fraction λ_0 of which lie in the same layer and a fraction λ_1 of which lie in each of the adjacent layers. A polymer molecule is represented by a chain of r_i connected segments, numbered $s=1,2,\ldots,r^i$. The index i is adopted to denote the type of the molecule. An additional index j is used in order to account for the polydispersity. Thus, chains appear with several sizes, r_j^i, where j varies from a minimum to a maximum value. From two consecutive segments we define the bond, b (b(of segments s)$\equiv b_s=z_s-z_{s-1}$). For two consecutive segments lying in layers z and $z+1$, b is $+1$. For two consecutive segments lying in layers z and $z-1$, b is -1. The value of b is 0 if both consecutive segments are lying in layer z.

Each chain can assume a large number of possible conformations in the lattice. Each conformation (c) is defined by specifying the layer numbers in which each of the successive chain segments s finds itself (i.e. $c\equiv\{(s=1,\ z=z_1),\ (s=2,\ z=z_2),\ldots,(s=r_j^i,\ z=z_{r_j^i})\}$). The number of chains (i, j) in conformation c is indicated as $n^c_{(i,j)}$. The chains are distributed over the various possible configurations (sets of conformations $\{n^c_{(i,j)}\}$) in the lattice with statistical weights depending on the energy and entropy of each configuration. The proper description of the system will be given in the context of statistical physics by means of the grand canonical partition function. The non-bonded chain interactions are approximated using the Bragg–Williams mean field approximation and the intra-chain interactions are approximated using bending energies. Equilibrium is the state at which the chains are distributed over the various possible conformations in the lattice such that the free energy (derived from the partition function) is at its minimum. In the mean field approximation, we make the assumption of replacing the sum of several terms in the partition function by its maximum term (i.e. zero fluctuations of the density in the (x, y) directions). An expression for the number of molecules $n^c_{(i,j)}$ of chain type i of size r_j^i in conformation c, can be found by minimizing the natural logarithm of the maximum term of the partition function with respect to $n^c_{(i,j)}$, subject to the full occupancy constraint applied layerwise.

In order to develop a theoretical framework capable of describing realistic situations, the initial version of the SCF theory has been extended to incorporate conformational stiffness [45–48]. Chain stiffness is introduced by assigning different bending energies to different bending angles formed by triplets of segments (or pairs of bonds). For a cubic lattice only 0° (back folding or V conformer), 90° (L conformer) and 180° (straight or I conformer) bending angles are possible (see Fig. 2 in Ref. [48]). The bending energies can be determined from the characteristic ratios [47–49]. To each bending energy (ε_b) we associate the corresponding Boltzmann factor $\tau_b=\exp(-\varepsilon_b/k_BT)$, where T is the temperature.

The system can be described in a mean field self-consistent approximation in terms of a segment potential $u_A(z)$ depending only on the chemical nature of the segment, or equivalently in terms of a segment weighting factor $G(z)=e^{-u_A(z)/kT}$. The weight $G(z)$ is proportional to the probability of finding a segment in layer z of the interfacial system, relative to finding it in the bulk. Then the statistical weight for finding an end of an s-segment long chain in layer z, $G(z, s)$, is defined. It follows a recursion relation, which is solved once we know a proper initial condition. For the

forward propagation the recursion relation has the following expression:

$$G^{b_s}(z,s|1) = G(z)\langle G^{b_{s-1}}(z-b_s, s-1|1)\rangle \tag{1}$$

where

$$\langle G^{b_{s-1}}(z-b_s,s-1|1)\rangle \equiv \lambda_{|b_s|}\sum_{b_{s-1}} \tau_{b_{s-1}b_s} G^{b_{s-1}} \times (z-b_s, s-1|1) \tag{1'}$$

For the backward propagation:

$$G^{b_s}(z,s|r) = G(z)\langle G^{b_{s+2}}(z+b_{s+1}, s+1|r)\rangle \tag{2}$$

where

$$\langle G^{b_{s+2}}(z+b_{s+1},s+1|r)\rangle \equiv \lambda_{|b_{s+1}|}\sum_{b_{s+2}} \tau_{b_{s+1}b_{s+2}} G^{b_{s+2}}(z+b_{s+1}, s+1|r) \tag{2'}$$

Then by means of a composition law we find the volume fractions. For the grafted chains:

$$\phi(z) = G(z)^{-1}\sum_{s=1}^{r^g_{\max}}\sum_{b_s}\sum_{b_{s+1}} \tau_{b_s b_{s+1}} G_g^{b_s}(z,s/1) \times \left[C_s^g G_g^{b_{s+1}}(z,s/s) + G_g^{b_{s+1}}(z,s/\{k\geq s+1\})\right] \tag{3}$$

where $C_s^g = \tilde{\sigma}(n_s^g/n_{\text{total}}^g)1/\sum_z G_g(z,s/1)$ and $\tilde{\sigma}$ is the dimensionless surface density.

The solvent's volume fraction is:

$$\phi(z) = C_1^{\text{f}} G(z) \tag{3'}$$

where $C_1^{\text{f}} = (M - \bar{r}^g\tilde{\sigma})/\sum_z G(z)$. M is the number of the layers.

Finally, it is straightforward to find the concentration of the end and non-terminal segments.

The details of the SCF formalism are given in Refs. [32–35,47,48]. From now on, this modified version of the plain SCF theory, which treats both features (polydispersity and end-grafted chains) simultaneously, will be referred as numerical SCF (nSCF) theory.

Actually, all equations derived for melts in Ref. [48] are valid. But in melt polymer brush we impose the constraint that the lattice is fully occupied exclusively by grafted chains. Hence, the number of layers, M is given by: $M = \bar{r}^g\tilde{\sigma}$, where $\bar{r}^g$ are the number-average molecular weight of the grafted chains. In the present work, we use M' layers with $M' > M$, so the $(M'-M)$ layers are occupied by solvent molecules, where each solvent molecule occupies one lattice site.

In order to describe bidisperse brushes in a good solvent, Zhulina et al. [20] have derived the following analytical expressions for the height of the two characteristic regions of the bimodal brushes.

$$H_{\text{S}} = H_{\text{o}}\sqrt{1-\tilde{q}^{2/3}} \tag{4a}$$

$$H_{\text{L}} = H_{\text{o}}(1+\alpha\tilde{q}^{1/3}) \tag{4b}$$

where $\alpha \equiv (N_{\text{L}} - N_{\text{S}})/N_{\text{S}}$

The short and the long chains consist of N_{S} and N_{L} segments, respectively. The symbol $\tilde{q}$ is the percentage of the long chains, while H_{o} is the height of the monodisperse case with the same dimensionless surface density $\tilde{\sigma}$.

$$H_{\text{o}} = \beta\tilde{\sigma}^{1/3}N_{\text{S}} \tag{4c}$$

The parameter β symbolize the stiffness p and the quality υ (second virial coefficient) of the good solvent, $\beta \equiv (8p\upsilon/\pi^2)^{1/3}$. According to this theory, the bi-parabolic volume fraction profile is given by the following expressions:

$$\phi(z) = \frac{3}{2}\tilde{\sigma}^{2/3}\left(\frac{\pi^2 a^3}{8p\upsilon}\right)^{1/3}\left(1-\left(\frac{z}{H_{\text{o}}}\right)^2\right), \quad 0\leq z\leq H_s \tag{5a}$$

$$\phi(z) = \frac{3}{2}\tilde{\sigma}^{2/3}\left(\frac{\pi^2 a^3}{8p\upsilon}\right)^{1/3}\left(1-u^2\left(\frac{z}{H_{\text{o}}}\right)\right), \quad H_s\leq z\leq H_{\text{L}} \tag{5b}$$

where $u(x) = (x - \alpha[x^2 - (1-\alpha^2)(1-\tilde{q}^{2/3})]^{1/2})/(1-\alpha^2)$ and a^3 is the monomer's volume.

2.1. Mapping real polymers onto the lattice

Among the possible choices for the lattice segment size, the ones that have been used the most are the Kuhn statistical segments [48,53] and the Flory segments [47–50]. A Flory segment, of length l_{F}, is defined such that a chain will have the same maximally extended length (end-to-end distance in all-*trans* conformation) and volume in the Flory segment representation as are measured experimentally in polymer melts [47,48].

Equating the volume of the Flory chain, containing r Flory segments, to the volume of a real chain:

$$rl_{\text{F}}^3 = \frac{n_{\text{m}}M_{\text{m}}}{N_{\text{A}}\rho} \tag{6a}$$

where n_{m} is the degree of polymerization, M_{m} is the monomer molecular weight, ρ the mass density of the polymer and $N_{\text{A}}$is Avogadro's number.

Moreover, equating the length of the fully extended Flory chain to the maximally extended length of the real chain:

$$rl_{\text{F}} = n_{\text{b}}l_{\text{b}}\sin\left(\frac{\theta_{\text{b}}}{2}\right) \tag{6b}$$

where n_{b} is the number of chemical bonds per chain, l_{b} is the bond length and θ_{b} is the bond angle along the chain backbone.

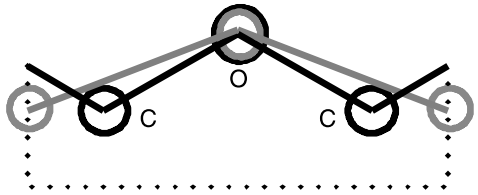

Scheme 1. Geometrical mapping of a PEO monomer (atoms and bonds in black) onto an equivalent three-bead 'polymethylene' monomer ('atoms' and 'bonds' in grey).

By combining these equations, an expression for the length of the Flory segment is obtained,

$$l_F = \left[\frac{n_m M_m}{N_A \rho n_b l_b \sin\left(\frac{\theta_b}{2}\right)}\right]^{1/2} \quad (7)$$

The bending energies are determined from the characteristic ratios by matching the mean-square end-to-end distance between a real chain and a chain of correlated Flory segments,

$$\langle R^2 \rangle = C_\infty n_b l_b^2 = C_\infty^F (r-1) l_F^2 \quad (8a)$$

in which C_∞^F is the characteristic ratio of the correlated Flory chain.

Assuming that $\tau_V = 0$ (i.e. back-folding is forbidden), the characteristic ratio of the Flory chain is related to the bending statistical weights by

$$C_\infty^F = 1 + \frac{\tau_I}{2\tau_L} = 1 + \frac{1}{2} e^{(\varepsilon_L - \varepsilon_I)/kT} \quad (8b)$$

Since the characteristic ratio depends only on the difference between the energies $(\varepsilon_L - \varepsilon_I)$, one (in our case ε_I) case may be set arbitrarily to zero. So the bending energy ε_L can be estimated once the characteristic ratio C_∞ is known.

The Flory segment is usually much shorter than the Kuhn segment. Most researchers use the Kuhn segment as the unit segment for their coarse-grained representation. In our nSCF methodology, we use the Flory segments, in order to have correct representation of both polymer density and polymer stiffness and hence study realistic polymer systems [49–51].

3. Brushes studied by neutron reflectivity

3.1. PS in good solvent

Our theoretical investigation starts with the polymeric brush studied by Kent et al. [25]. The system investigated consisted of Langmuir monolayers of highly asymmetric poly(dimethylsiloxane)–polystyrene (PDMS–PS) diblock copolymers on the interface of air–ethylbenzoate (EB). This is a system with the smaller PDMS blocks (physically) anchored to the interface creating Langmuir monolayers. To our knowledge, this experimental study was the first direct measurement of the structure of bimodal tethered chain layer using neutron reflectivity. In our computational model we treat this system as a system of grafted chains, as the anchoring energies are very large [25].

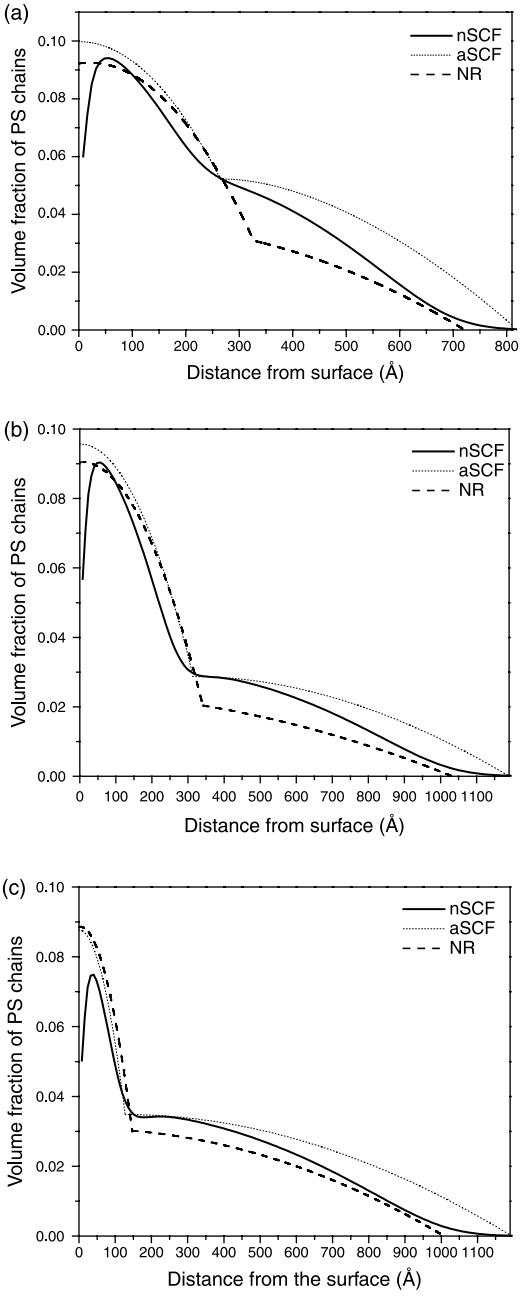

Fig. 1. Volume fraction profiles of PS chains as a function of the distance from the interface, for bimodal monolayers. The solid line describes the prediction of nSCF model and the dashed line the best-fit to the experiment [25]. Doted lines depict the predictions of the aSCF theory [20]. The systems studied are: (a) 66/170 kg/mol, $\sigma = 2\times10^{-2}$ chains/nm^2, 62% short chains. (b) 66/330 kg/mol, $\sigma = 1.88\times10^{-2}$ chains/nm^2, 83% short chains. (c) 30/330 kg/mol, $\sigma = 1.75\times10^{-2}$ chains/nm^2, 75% short chains.

The mapping of the experimental system to our lattice SCF system is straight forward (i.e. we use the Flory segments, Section 2.1). In the results produced by means of

our nSCF method, we have assumed that the temperature of our system is 25 °C, which is the temperature at which experimental data [25] were collected. We use a mass density of 1.0525 g/cm^3; a value derived from expressions, of the mass density as a function of the pressure and temperature, found in Ref. [52]. The Flory segment estimated as $l_F = 8.016$ Å, therefore, the number of chemical (styrene) monomers in a Flory segment is 3.14. The value used in the present work for the characteristic ratio, C_∞, of the equivalent trimer was estimated to be 8.00 [52,53]. For this C_∞, Eqs. (8a) and (8b) give a bending energy $\varepsilon_L = 0.538 k_B T (\tau_L = 0.584)$.

Practically, the only parameter in our system is the Flory interaction parameter between the PS and the good solvent. We assume that PS polymeric chains and solvent have approximately the same interaction energy with the interface hence they show a zero Flory interaction parameter. The best choice for the Flory parameter for the interaction between polystyrene and the EB solvent (a good solvent for PS) is $\chi = 0.15$. We have studied all bidisperse systems investigated by Kent et al. [25]. Therefore, our systematic study includes diblock bimodal copolymers PDMS–PS of molecular weights 11–66/20–170, 11–66/28–330 and 4–30/28–330 kg/mol. In order to compare with the aSCF predictions we need to estimate the β parameter. This is done by identifying the Flory segment of the nSCF theory with the a-parameter of the aSCF theory. Then, the parameter β takes the value 0.811 nm (i.e. 1.012 Flory segments).

3.2. PEO in good solvent

The second system investigated consists of diblock copolymer polystyrene–poly(ethyl oxide) (PS–PEO). The system has been studied with NR by Currie et al. [27]. The block copolymers were dissolved in chloroform and deposited on a air-water interface. The smaller PS blocks anchor the copolymers to the interface. This system has also been treated as a system of grafted chains.

Since the bonds C–O and C–C do not have the same length we map the PEO monomer onto an equivalent 'polyethylene trimmer' (Scheme 1) [49]. This equivalent structure contains only single bonds, each with bond length of $l_b = 1.96$ Å and angle between the two successive bonds, θ_b, at 131°.

In the results produced by means of our nSCF method, we have assumed that the temperature of our system is 25 °C, which is the temperature at which experimental data [27] were collected. The mass density is 1.10 g/cm^3; found in Ref. [52]. The Flory segment estimated as $l_F = 4.315$ Å, therefore, the number of chemical (ethyl oxide) monomers in a Flory segment is 1.21. The value used for the characteristic ratio, C_∞, was estimated to be 3.4 [52,53]. For this C_∞, Eqs. (8a) and (8b) give a bending energy $\varepsilon_L = -2.45\ k_B T (\tau_L = 11.593)$.

The optimum choice for the Flory interaction parameter between the PEO and the good solvent (D_2O) is $\chi = 0.12$. In Ref. [28] an analogue investigation with SCF theory proposed $\chi = 0$. This difference is legitimate since with our nSCF we account for the chain stiffness too. We assume that PEO polymeric chains and solvent have a difference in the interaction energy with the interface approximately $1 k_B T$. Hence the Flory interaction parameter between the PEO and interface is $\chi = -1$ (the minus sing shows that there is a preference for the surface).

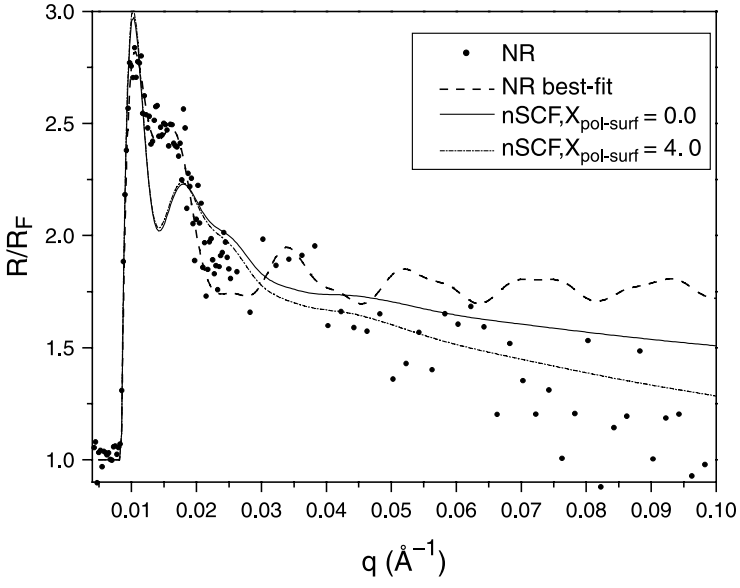

Fig. 2. Reflectivity divided by reflectivity for bare EB surface for the case of Fig. 1(a). We present the predictions of the nSCF theory (solid line) and the best-fit to NR data (dashed line). The worst agreement is observed for q-values in a region around 0.015 Å^{-1}. At high values of q (>0.03 Å^{-1}), the agreement is much better than the best-fit to NR data. Moreover if we set a non-zero value in the adsorption energy of the polymer, at about $4kT$, we achieve even better agreement at this region of q (doted line).

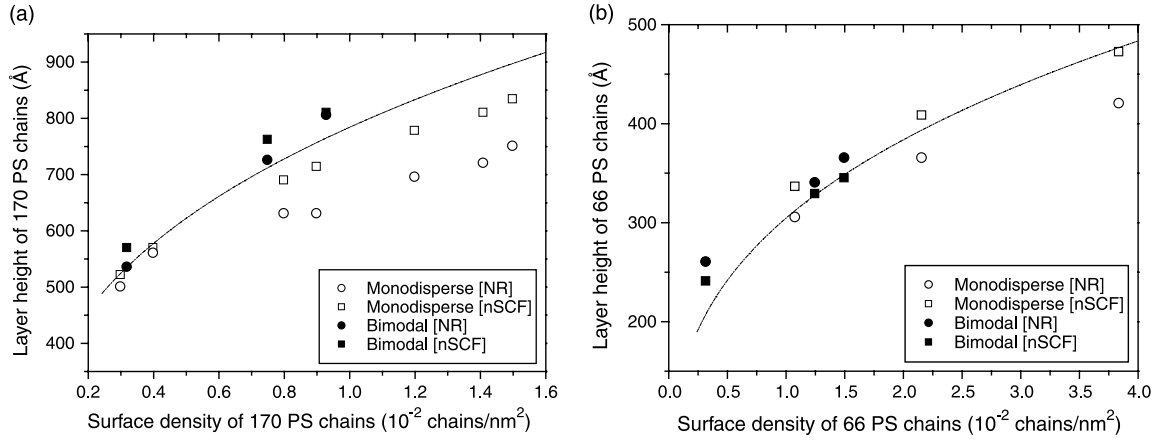

Fig. 3. Plots of the layer heights, as a function of the surface density, of the 66 and 170 K PS blocks. (a) Comparison of the layer heights of the 170 PS blocks in the mixed monolayers (filled symbols) with those in the single component 170 monolayers (open symbols) as a function of 170 surface density. In the strongly interacting regime, the 170 blocks are more stretched in the bimodal monolayer than in the single-component monolayers. (b) Comparison of the layer heights of the 66 PS blocks in the mixed monolayers (filled symbols) with those in the single component 66 monolayers (open symbols) as a function of 66 surface density. In the strongly interacting regime, the 66 blocks have nearly the same dimension in the bimodal monolayer as in the single-component monolayers. In both plots the circles correspond to the NR data and the squares to the nSCF results. Dashed lines depict the predictions of the aSCF theory [20] for the single component case.

4. Results and discussion

In Figs. 1–3, we show results for the PS and we compared with the experimental data from NR experiments. Fig. 1 shows volume fraction profiles for the bimodal systems studied experimentally in Ref. [25]. The systems investigated include various surface densities of the anchoring blocks and percentages of the short chains. In Section 4, we report experimental surface density in units of inverse surface. The relation between this surface density and the dimensionless one used in the expressions of the nSCF and aSCF models is $\tilde{\sigma} = \sigma l_F^2$. In Fig. 1(a), we study the 66/170 kg/mol system with surface density of the anchoring blocks $\sigma = 0.02$ chains/nm^2, where the percentage of the short chains is about 62%. In Fig. 1(b) and (c), we investigate the 66/330 kg/mol system with $\sigma = 1.88 \times 10^{-2}$ nm^{-2} and 83% short chains and the 30/330 kg/mol system with $\sigma = 1.65 \times 10^{-2}$ nm^{-2} and 75% short chains, respectively. Generally the agreement between nSCF and best-fit to NR data profiles is very satisfactory (in our work we use the same Flory interaction parameter for all existing experimental data). In the same figure, we plot the predictions of the aSCF methodology [20], where similar behavior is observed. The most significant deviation of the SCF theory, in both numerical and analytical form, from the best-fit to NR data profiles, is observed in Fig. 1(a).

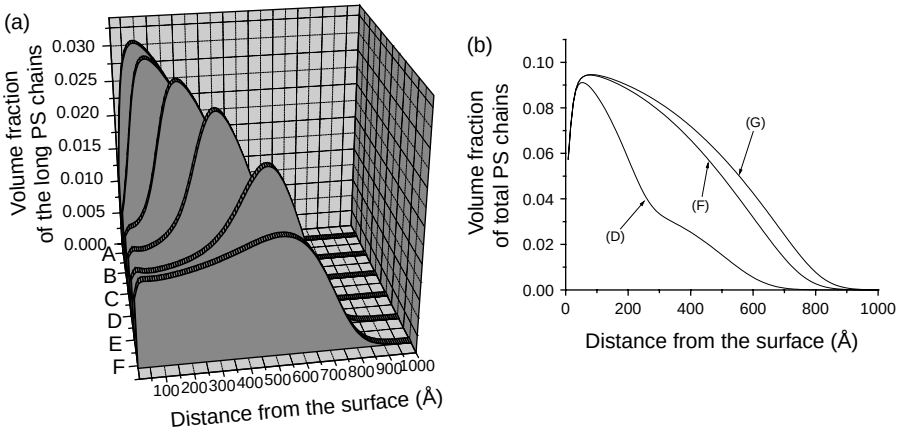

Fig. 4. Volume fraction profiles of PS bimodal brushes. (a) The influence of the size of the short chains on the stretching of the long chains is systematically studied by assuming various molecular weights for the short PS chains. Graph A presents the monodisperse case (170 kg/mol) with $\sigma = 0.38 \times 10^{-2}$ chains/nm^2. In all other graphs we keep fixed the molecular weight of the long chains (170 kg/mol), the total surface density ($\sigma = 1.9 \times 10^{-2}$ chains/nm^2) and the proportion of the long chains (1/5). Short chains molecular weight (in kg/mol) grows gradually (B:8.2, C:32.7, D:66, E:117.8, F:150.3). Graph F indicates that when short chains become almost 85% the size of the long, the stretching of the long and short chains is very similar resulting in almost mono-parabolic profile. (b) The volume fraction for the graph F resembles the monodisperse case (short chains with molecular weight of 170 kg/mol and $\sigma = 1.9 \times 10^{-2}$ chains/nm^2), which is plotted in graph G.

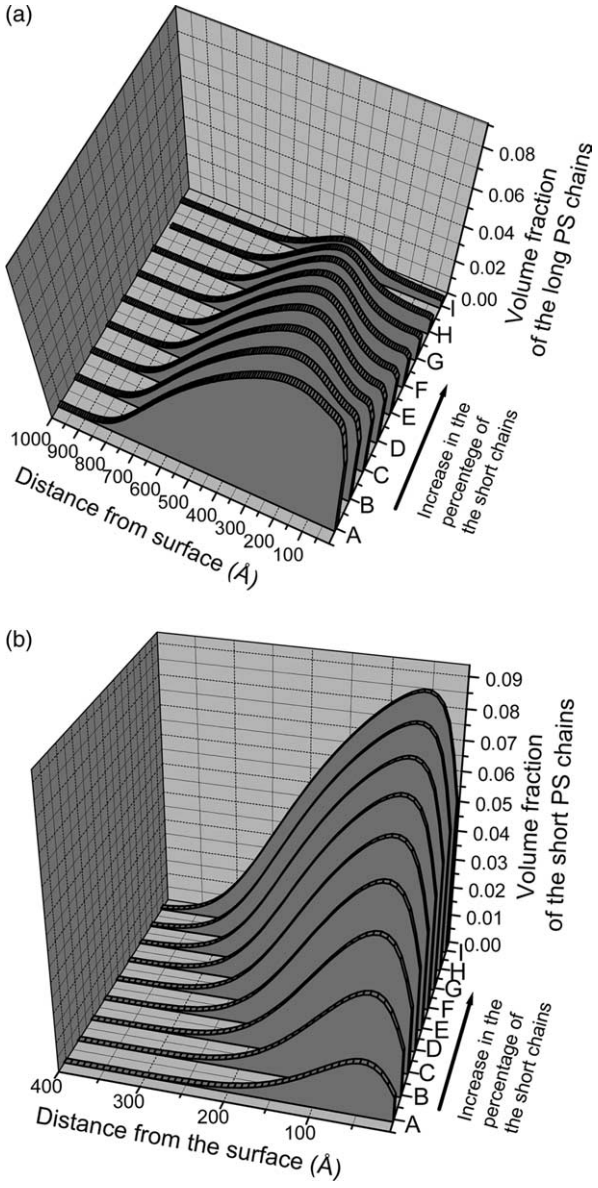

Fig. 5. Volume fraction profiles of the long (a) and short (b) chains as a function of the distance from the surface for 66/170 kg/mol bimodal system. The percentage of the short chains increases from 10% (graph A) to 90% (graph I) with constant rate. The total surface density is constant ($\sigma = 1.9\times10^{-2}$ chains/nm^2).

Then we have estimated the reflectivity spectrum of each system under investigation. Fig. 2 shows that the agreement is satisfactory, with largest deviation in the region 0.012–0.02 Å^{-1}. Moreover, we have found that the agreement with reflectivity data is even better if we assume a repulsive force between the surface and the polymeric material (PS). If the Flory interaction parameter between the PS and the interface is set to 4, the corresponding reflectivity from the nSCF volume fraction profile matches better the NR data for high values of the scattering vector q (dotted line in Fig. 2).

Next in Fig. 3, we compare the characteristic dimensions of the bimodal structure with those of the single-component monolayers. Such a comparison requires the knowledge of

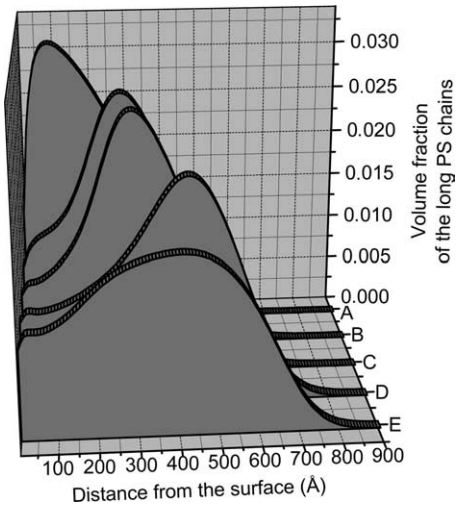

Fig. 6. Volume fraction profiles of the long PS chains as a function of the distance from the surface for trimodal brushes. The size of the long chains (170 kg/mol), the total surface density ($\sigma = 1.9\times10^{-2}$ chains/nm^2) and the percentage of the long chains (20%) are kept constant. Graph A presents the monodisperse case (170 kg/mol) hence $\sigma = 0.38\times10^{-2}$ chains/nm^2. For the shorter chains, one chain size is kept constant (66 kg/mol) while the molecular weight (in kg/mol) of the other chain grows gradually (B:8.2, C: 32.7, D:114,4, E:150.3). The trimodal mixture consists of 40% medium size chains and 40% short chains. Graph E shows that as medium chains become larger, an analogue effect as those observed for the bimodal case is present, where the stretching of the long and short chains tends to be similar.

the surface density of each component in the mixed monolayer. In our computational study we have used the estimations for the surface density, derived in the experimental NR study [25]. In Ref. [25], in order to estimate the surface densities they have made the assumption that the profiles of the bimodal (mixed) monolayer can be resolved into two parabolas representing the contributions of the two components. The filled symbols in both Fig. 3(a) and (b) are referred to three bimodal systems with the same molecular weight of 66/170 kg/mol but different surface densities and percentage of short chains. The overall surface densities, with increasing order, are $\sigma = 0.62\times10^{-2}$ nm^{-2}, $\sigma = 2\times10^{-2}$ nm^{-2} and $\sigma = 2.43\times10^{-2}$ nm^{-2}. In the first case the percentage of the short chains is 50% and in the other two cases the percentage of the short chains is 62%.

We show data on the layer height for various surface densities of the single-component and of the mixed monolayer. In Fig. 3(a), we compare our results (square symbols) for the layer height of the 170 PS blocks in the 11–66/20–170 mixed monolayers with those in the single-component 20–170 monolayers as a function of 20–170 surface density. We clearly observe that in the strongly interacting regime, the 170 blocks are more stretched in the bimodal monolayer, than in the single-component monolayers. On the contrary when we compare in Fig. 3(b) the layer heights of the 66 PS blocks in the 11–66/20–170 mixed monolayer with those in the single-component 11–66 monolayer as a function of 11–66 surface density, we

observe that even in the strongly interacting regime, the 66 blocks have nearly the same dimension in the bimodal monolayer as in the single-component monolayers. In order to understand the observed behavior we point out that in the first layer of the bimodal brush the contacts between the chains are reduced by the strong stretching of the long, while short chains are not disturbed appreciably. Moreover, in this way large part of the long chains is transferred to the outer region where the polymer concentration is lower and so the reduction of the entropy is much lower. In this way the system manages to minimize the free energy. This 'unexpected' increase (compared to the monodisperse case) of the polymer concentration in the outer region, is responsible for the bi-parabolic profile of the volume fraction of the polymer. From Fig. 3, we conclude that the same trends are observed from the NR experimental data and the nSCF calculated results.

In Fig. 4, we have also systematically study the influence of the molecular weight of the short chains on the extension of the long chains, assuming fixed surface density of each component of the bimodal system. We have found that the larger the size of the short chain the more extended are the long chains in the region close to the interface. But there is a maximum size of the short compared to the size of the long chains, where the minimization of the free energy is achieved by similar stretching of long and short chains. This is shown in graph F of Fig. 4(a) and more clearly in Fig. 4(b) where in the volume fraction profile of total PS chains we do not observe two parabolas. In this case, different stretching of the long compared to the short chains is not compensated by an entropic and enthalpic gain in the outer region where mainly long chains exist. So both long and short chains stretch similarly as in the monodisperse case (Fig. 4(b), graph G). From Fig. 4(b), we conclude that the maximum extension of the brush is achieved when short and long chains become of equal size (monodispere sample).

In addition, in Fig. 5 we have fixed the molecular weight and the total surface density and systematically increase the percentage of short chains. We observe an increase in the difference in the stretching of the long chains compared to the short chains as the percentage of the short chains in the bimodal mixture increases (Fig. 5(a)). In Fig. 5(b) we have shown that in the case of low percentage of short chains, the short chains shrink in proportion to the fraction of the short chains. Both conclusions agree with the predictions of the theoretical study of Dan and Tirrel [23].

Moreover, we have systematically investigated brushes with trimodal molecular weight distribution. Fig. 6 is a graphical presentation of the influence of the shorter chains on the stretching of the long chain. We concluded that one can find trimodal polymeric structures for which the longer chains behave as in the bimodal case where the stretched region next to the surface is maximized. In Fig. 7(a) we observe that for molecular weights 170/57/113 kg/mol (case of most extended trimodal brush) with 10% chains of 57 kg/mol and 70% chains of the intermediate molecular weight (113 kg/mol)

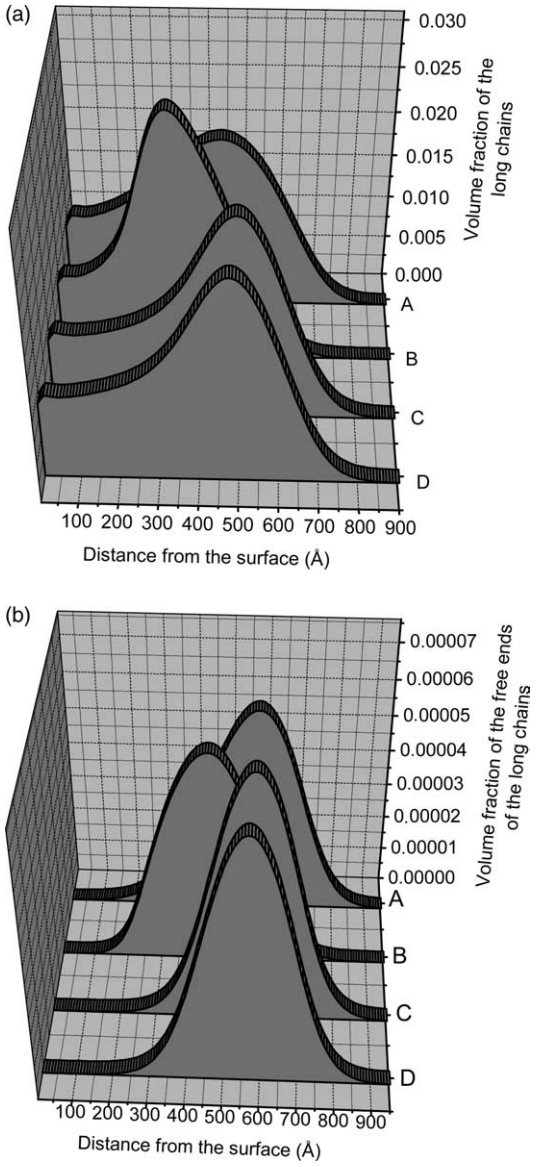

Fig. 7. Comparison of the trimodal case 170/113/56.5 kg/mol (showing the maximum stretching in the region close to the interface and brush height) with other polydisperse cases. In all cases long chains (170 kg/mol) represent 20% of the total surface density ($\sigma = 1.9 \times 10^{-2}$ chains/nm^2). Graph A corresponds to uniform distribution of the shorter chains (from 56.5 kg/mol to 169.6 kg/mol, at 80%). Graphs B and C depict bimodal cases where short chains sizes are 56.5 and 113 kg/mol, respectively. Graph D corresponds to trimodal distribution, where 70% are medium size chains and 10% short chains. (a) Volume fraction profiles of the long PS chains and (b) volume fraction profiles of the free ends of the long PS chains as a function of the distance from the surface for trimodal brushes.

we get a maximum at 480 Å comparing to the 304 Å for the bimodal case of 170/57 kg/mol when 80% of the chains are short chains. Moreover, the volume fraction of the free end-segments of long chains for the molecular weight 170/57/113 kg/mol maximizes at 561 Å, comparing to the bimodal case of 170/57 kg/mol where we get maximum at 416 Å and with slighter lower value (Fig. 7(b)). Graph C, in Figs. 7(a) and (b) indicates that the case of maximum stretching is

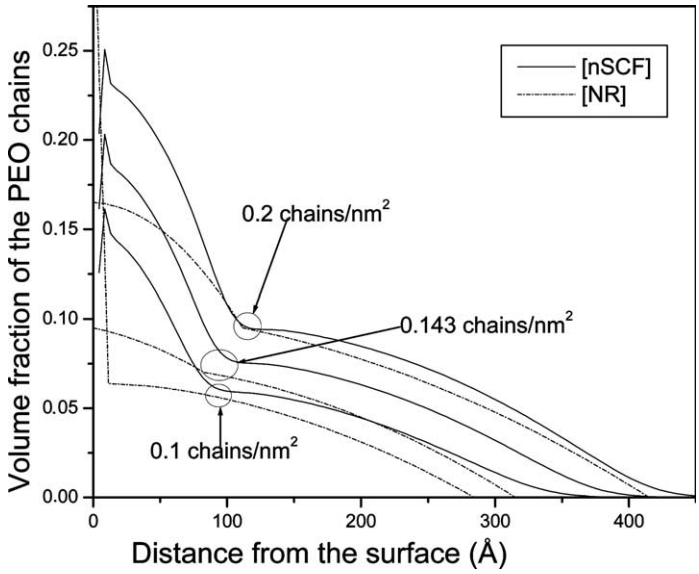

Fig. 8. Volume fraction profiles of PEO chains for bimodal distributions. The solid line describes the prediction of nSCF model and the dashed line the best-fit to the experiment [27]. The bimodal systems studied contain chains with molecular weights of 30.8 and 6.6 kg/mol. The percentage of the short chains is 75%. We present three cases with different surface densities (σ). The χ parameter for the interaction between surface and polymer is -1.

when short chains reach the size of the medium size chains, i.e. when the trimodal distribution collapses to a bimodal distribution (170/113 kg/mol).

We complete our study with a systematic investigation of the PEO solution. Our investigations have shown that for this solution it is necessary to assume an interaction parameter between polymer and surface, different from the interaction parameter between solvent and surface. In Fig. 8, we reproduced three volume fraction profiles corresponding to three different surface densities of the 6.6/30.8 kg/mol bimodal system. Our nSCF results are compared with NR experimental data, as the three cases studied are the ones studied by NR experiments in Ref. [27]. The curve for surface density of 0.2 nm^{-2} shows very good agreement with the second parabola of the experimental fit. However, near the surface there is an important deviation. As surface density degrease, deviations from the experimental results become more pronounced. Similar results have been obtained with previous numerical SCF method [27] (in which the polymer stiffness is not taken into account), where, actually, the deviations between theoretical and experimental results were much larger [27]. We

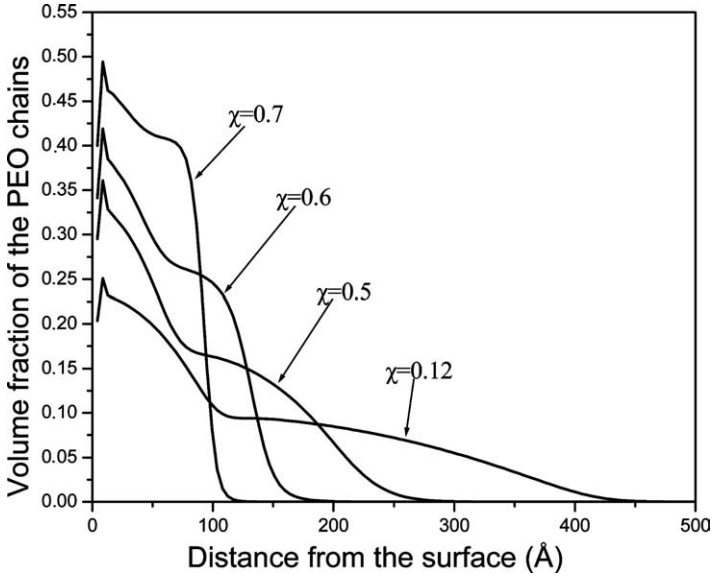

Fig. 9. Volume fraction profiles of PEO for various values of the interaction parameter between polymer and solvent χ. The system studied consists of chains with molecular weights 30.8 and 6.6 kg/mol, the percentage of the short chains is 75% and $\sigma = 0.2$ chains/nm^2. Increase of χ causes shrinkage of the brush and an significant deviation from bi-parabolic profile. The parameter for the interaction between surface and polymer is -1.

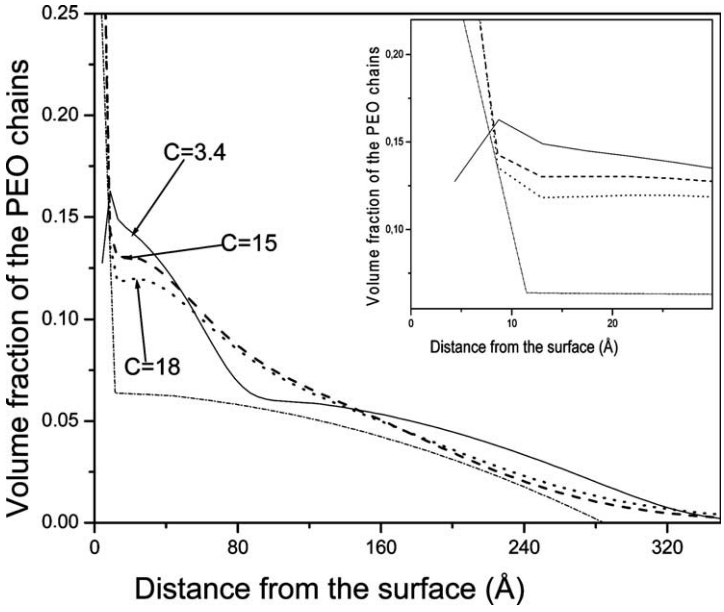

Fig. 10. Volume fraction profiles of PEO for low surface density (0.1 chains/nm^2) for various characteristic ratios. For $C_\infty = 3.4$ (solid line) the system is the same as those presented in Fig. 8 ($\chi = 0.12$). For higher values of characteristic ratios, $C_\infty = 15$ (dash line) and $C_\infty = 18$ (dot line) the interaction parameter is assumed to have higher value, $\chi = 0.5$, in order to describe the hydrophobic behaviour of PEO for this surface density. As C_∞ increases we observe a much better agreement between the experimental and calculated polymer volume fraction close to the surface, where the bi-parabolic profile is vanished. At even higher values of C_∞ the 'sudden' reduction of the polymer volume fraction very close to the surface is described even better. The results from NR are presented with dashed-dotted line.

believe, the reason for the observed differences between calculated and experimentally observed results is the existence of specific interactions (as for example Hydrogen bonding) between monomer (ethyl-oxide) and solvent (water) and between polymer and solvent and the air–water interface. For these cases the mean-field approximation of a stable-solvent solution is a reasonable approximation, only for a very narrow region of polymer surface density.

For the case with surface density of 0.2 nm^{-2}, at which our results are satisfactory, we present a systematic investigation for other type of solvents. In Fig. 9 we confirm a shrinking of the brush as contacts with solvent become unfavorable (bad solvent). The shrinkage effect is enormous as we increase the interaction parameter, so that for $\chi = 0.7$ the bi-parabolic profile practically disappears. Very similar effects were observed for the PS chains dissolved in various solvents (not shown).

Finally, we have tried to explain the observed behavior for the lowest surface density case. In this case, the experimentalists suggest one parabolic profile for the volume fraction profile of the polymer [27]. By systematically studying this case, assuming various characteristic ratios, we have found that the best agreement between the nSCF results and the NR profiles is achieved for higher values of the characteristic ratio and the interaction parameter between solvent and polymer ($\chi \sim 0.5$) (Fig. 10). In order to explain this increase of the stiffness and the change in the solubility of the macromolecule, we exploit the hydrophobic behavior of the PEO. For low surface densities (for example for surface density of 0.1 nm^{-2}) the average distance between the grafting points is so large that practically each macromolecular chain is surrounded by mainly water molecules. Hence each macromolecule is encaged by water molecules [54] and effectively acquires a rod-like conformation. Thus it shows an effective very high characteristic ratio. Moreover as shown by the NR results, the polymer concentration is very high on the surface and drops abruptly. This behavior can be explained by the acceptance of almost bad solvent and a very stiff 'diluted' polymer chain (hydrophobic hydration, [54]). Actually, we have found that for large values of the characteristic ratio, the agreement between the nSCF estimated volume fraction profiles and the NR estimated profiles is very good for the low (0.1 nm^{-2}) surface density case (Fig. 10).

5. Conclusions

We have systematically studied a poly-disperse polymer brush dissolved in a good solvent by applying a recently developed lattice-based self-consistent mean field theory. Bimodal and trimodal di-block structures were investigated. In all cases of PS brushes we have achieved very good agreement with the experimental results of Ref. [25]. Deviations between theory and experiment were noticed for the PEO for low concentrations, because of special interactions between monomer and solvent [27]. It worth pointing out that

our SCF methodology produces very good quantitative agreement. For some low surface densities, the PEO system does not show good agreement, which is attributed to the presence of specific interactions between polymer and solvent and polymer and surface. We have also systematically studied the structure of the bi-disperse and tri-disperse brush for various values of the molecular weights of the components and of the overall surface densities. For the bimodal brush we have found that the short chains even in the strongly interacting regime have nearly the same dimension in the bimodal nonolayer as in the single-component monolayers. This is not true for the long chains. Moreover, we have shown that in the trimodal brush the chains with the intermediate size can play an important role. Finally, we have found that when χ parameter, for the interaction between polymer and solvent, is bigger than 0.5 we observe a deviation from the bi-parabolic profile.

Acknowledgements

I would like to thank Dr M. Kent for providing us with the Reflectivity experimental data and Assistant Professor D. Anastassopoulos for helping us with the reflectivity calculations. Computational resources for this research were made available by the Educational and Initial Vocational Training Program on Polymer Science and Technology-3. 2a. 33H6. This work was supported by the Greek Secretariat for Research and Technology (GGET) by a grant (PENED 01ED529).

References

[1] Alexander SJ. J Phys (Paris) 1976;38:977.
[2] DeGennes P-G. Macromolecules 1980;13:1069.
[3] Milner ST. Science 1991;252:905.
[4] Halperin A, Tirrell M, Lodge TP. Adv Polym Sci 1992;100:31.
[5] Granick S. Polymers in confined environments. Berlin: Springer; 1999.
[6] Fleer GJ, Cohen Stuart MA, Scheutjens JMHM, Cosgrove T, Vincent B. Polymers at interfaces. Cambridge: Chapman and Hall; 1993.
[7] Auroy P, Auvray L, Leger L. J Phys: Condens Matter 1990;2:317.
[8] Auroy P, Mir Y, Auvray L. Phys Rev Lett 1992;69:93.
[9] Taunton HJ, Toprakcioglu C, Fetters LJ, Klein J. Nature 1988;332: 712.
[10] Taunton HJ, Toprakcioglu C, Fetters LJ, Klein J. Macromolecules 1990;23:571.
[11] Klein J, Perahia D, Warburg S. Nature 1991;352:143.
[12] Tirrell M, Patel S, Hadziioannou G. Proc Natl Acad Sci 1987;84:4725.
[13] Ansarifar MA, Luckham PF. Polymer 1988;29:329.
[14] Taunton HJ, Toprakcioglu C, Klein J. Macromolecules 1988;21:3333.
[15] Cosgrove T, Heath T, van Lent B, Leermakers F, Scheutjens JMHM. Macromolecules 1988;20:1692.
[16] Patel SS, Tirrell M. Annu Rev Phys Chem 1989;40:597.
[17] Jones RAL, Richards RW. Polymers at surfaces and interfaces. Cambridge: Cambridge University Press; 1999.
[18] Tirrell M, Parsonage E, Watanabe H, Dhoot S. Polym J 1991;23:641.
[19] Milner ST, Witten TA, Cates M. Macromolecules 1988;21:2610.
[20] Birshtein TM, Liatskaya YV, Zhulina EB. Polymer 1990;31:2185.
[21] Chakrabarti A, Toral R. Macromolecules 1990;23:2016.
[22] Lai PY, Zhulina EB. Macromolecules 1992;25:5201.
[23] Dan N, Tirrell M. Macromolecules 1993;26:6467.
[24] Amoskov VM, Birshtein TM. Macromolecules 2001;34:5331.
[25] (a) Kent MS, Factor BJ, Satija S, Gallagher P, Smith GS. Macromolecules 1996;29:2843.
(b) Kent MS. Macrommol Rapid Commun 2000;21:243.
[26] Kent MS, Lee LT, Factor BJ, Rondelez F, Smith GS. J Chem Phys 1995;103:2320.
[27] Currie EPK, Wagemaker M, Stuart MAC, van Well AA. Macromolecules 1999;32:9041.
[28] Currie EPK, Leermakers FAM, Cohen Stuart MA, Fleer GJ. Macromolecules 1999;32:487.
[29] Edwards SF. Proc Phys Soc (London) 1965;85:613.
[30] Dolan AK, Edwards SF. Proc R Soc (London) 1974;A337:509.
[31] Dolan AK, Edwards SF. Proc R Soc (London) 1975;A343:427.
[32] Scheutjens JMHM, Fleer GJ. J Phys Chem 1979;83:1619.
[33] Scheutjens JMHM, Fleer GJ. J Phys Chem 1980;84:178.
[34] Scheutjens JMHM, Fleer GJ. Macromolecules 1985;18:1882.
[35] Evers OA, Scheutjens JMHM, Fleer GJ. Macromolecules 1990;23: 5221.
[36] Netz RR, Schick M. Macromolecules 1998;31:5105.
[37] Milner ST. Europhys Lett 1988;7:695.
[38] Milner ST, Wang ZG, Witten TA. Macromolecules 1989;22:489.
[39] Birshtein TM, Lyatskaya YV, Zhulina EB. Polym Sci USSR 1990;32: 1626.
[40] Milner ST, Witten TA, Cates M. Macromolecules 1989;22:853.
[41] Zhulina EB, Borisov OV, Pryamitsyn VA, Birshtein TM. Macromolecules 1991;24:140.
[42] Zhulina EB, Borisov OV, Brombacher L. Macromolecules 1991;24: 4679.
[43] Lyatskaya YV, Leermakers FAM, Fleer GJ, Zhulina EB, Birshtein TM. Macromolecules 1995;28:3562.
[44] Birshtein TM, Amoskov VM. Polym Sci C (Russia) 2000;42:172.
[45] Theodorou DN. Macromolecules 1988;21:1400.
[46] Wijmans CM, Leermakers FAM, Fleer GJ. J Chem Phys 1994;101: 8214.
[47] Fischel LB, Theodorou DN. J Chem Soc Faraday Trans 1995;91: 2381.
[48] Terzis AF, Theodorou DN, Stroeks A. Macromolecules 2000;31:1312.
[49] Terzis AF. Polymer 2002;43:2444.
[50] Retsos H, Terzis AF, Anastadiadis SH, Anastasopoulos DL, Toprakcioglu C, Theodorou DN, et al. Macromolecules 2002;35:1116.
[51] Daoulas KC, Terzis AF, Mavrantzas VG. J Chem Phys 2002;116: 11028.
[52] (a) Mark JE. Physical properties of polymers handbook. WoodBury, NY: American Institute of Physics Press; 1996.
(b) Brandrup J, Immergut EH. Polymer handbook. 3rd ed. New York: Wiley; 1989.
[53] Mattice WL, Suter UW. Conformational theory of large molecules. New York: Wiley; 1994.
[54] Kjellander R, Florin E. J Chem Soc, Faraday Trans 1 1981;77: 2053.